CRYSTAL GROWTH & DESIGN

Article

Cite This: Cryst. Growth Des. XXXX, XXX, XXX−XXX

pubs.acs.org/crystal

Evidence of Low-Temperature Phase Transition in Tetracene−Tetracyanoquinodimethane Complex

Boris Averkiev,[†] Rohan Isaac,[‡] Evgheni V. Jucov,[†] Victor N. Khrustalev,[†,§] Christian Kloc,[∥] Laurie E. McNeil,[‡] and Tatiana V. Timofeeva*[,†]

[†]Department of Chemistry, New Mexico Highlands University, Las Vegas, New Mexico 87701, United States

[‡]Department of Physics and Astronomy, University of North Carolina - Chapel Hill, Chapel Hill, North Carolina 27599-3255, United States

[§]Peoples' Friendship University of Russia (RUDN), Moscow, 117198, Russia

[∥]School of Materials Science & Engineering, Nanyang Technological University, Singapore 639798, Singapore

Supporting Information

ABSTRACT: Multitemperature X-ray diffraction and vibrational spectroscopic studies of tetracene−tetracyanoquinodimethane (TCNQ) charge transfer cocrystals have revealed the existence of a reversible phase transition in the temperature interval 150−200 K. It was shown that a new monoclinic polymorph of the cocrystal exists above that temperature range, with a structure that is very similar to the one previously described in the literature as being triclinic. The crystal structures of the two polymorphs were also calculated with periodic density functional theory quantum chemical calculations, and their geometries were compared to the experimental ones. The degree of charge transfer in both polymorphs was characterized using alteration in the bond lengths of the TCNQ molecule and frequency shifts obtained from vibrational spectroscopy data.

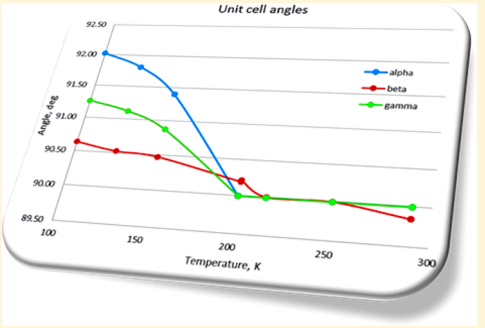

INTRODUCTION

Organic materials for photonics and electronics are in great demand since they have many properties that typically are not characteristic of inorganic electronic materials, such as lightweight, easy processability, flexibility, and biodegradability. Important for organic optoelectronics are charge transfer (CT) materials that can be employed in organic light emitting devices, photovoltaics, as field effect transistors, etc. The large variety of charge transfer materials includes organic polymers,[1] doped organic polymers,[2] individual small molecule compounds,[3] as well as doped small molecule materials[4] and binary (donor−acceptor)[5] or multicomponent small molecule adducts with different ratios of components.[6] It is known that the structural organization of the CT materials plays a crucial role in defining their properties. In crystal engineering, one of the tools to modify the structural characteristics of a crystalline material is to obtain different crystalline polymorphs. Examples of different binary CT polymorphs with different properties demonstrate the structure−properties dependence in CT materials.

Indeed, some binary CT crystals demonstrate several polymorphs with considerably different structures and properties. For instance, bis(ethylene-dithio) tetrathiafulvalene:tetracyanoquinodimethane (BEDT-TTF)−TCNQ crystallizes in two triclinic (β' and β'') and one monoclinic form. The two (BEDT-TTF)−TCNQ crystals built of stacks with alternating packing of D−A molecules (triclinic β' and the monoclinic phase) exhibit semiconducting properties, while the triclinic β'' phase with a segregated-stack packing demonstrates metallic behavior.[7]

Studies of two polymorphs of the binary complex of dibenzotetrathiafulvalene−7,7,8,8-tetracyanoquinodimethane (DBTTF−TCNQ) demonstrated that structural variations produce significant differences in optoelectronic properties of these crystals. The degree of charge transfer for one polymorph was about 0.5e, while in the second polymorph the molecules were almost neutral. This difference was related to the degree of overlap of donor and acceptor molecules in the crystals.[8]

It was shown that even small changes of molecular or crystal structure can affect its physical properties.[9] Such effects in crystals can be used for the materials whose physical properties can be externally controlled by electric field, temperature, pressure, etc. For example, it was demonstrated that the temperature dependence of the electrical characteristics of the complex *trans*-stilbene—2,3,5,6-tetrafluoro-7,7,8,8-tetracyanoquinodimethane (STB−F4TCNQ) is caused by the phase transition (order−disorder) in the crystal,[10] at which the overall molecular structure does not change, but the orientation disorder of the central C═C stilbene moiety occurs. The small shift of molecules in CT crystal can also be

Received: April 3, 2018
Revised: May 21, 2018
Published: June 5, 2018

DOI: 10.1021/acs.cgd.8b00501
Cryst. Growth Des. XXXX, XXX, XXX−XXX

responsible for its magnetic properties.[11] Such behavior was studied for crystals of tetrathiafulvalene (TTF) complexes with *p*-bromanil (tetrabromo-*p*-benzoquinone; BA) and *p*-chloranil (tetrachloro-*p*-benzoquinone; CA).

On the other hand, crystalline radical salts of (BEDT-TTF) with the monoanion tcnoetOH$^-$ (=$[(NC)_2CC(OCH_2CH_2OH)C(CN)_2]^-$) demonstrated two polymorphs with similar physical properties but different crystal packings. In should be mentioned that both polymorphs have alternating cationic and anionic layers, but the structure of these layers is different in the two polymorphs.[12] In this case, both polymorphs were obtained from solution under same conditions. Usually a change of preparation conditions causes the formation of different polymorphs; however, concomitant polymorphs also are observed in a significant number of cases.[13] There is as yet no consensus on what aspects of the crystal packing are most influential in determining the physical properties of the material. Accumulation of new experimental data is needed for a complete understanding of structure−properties interconnections for such materials. For this purpose, consideration of packing polymorphs of CT materials is especially important since they have the same molecular building units, and the only variable is the packing of these units in the crystals.

In this project we carried out experimental X-ray diffraction and spectroscopic multitemperature studies of the tetracene−tetracyanoquinodimethane (TCNQ) CT cocrystal (Scheme 1). Its low-temperature *triclinic* structure was reported

Scheme 1. Tetracene−7,7,8,8-tetracyanoquinodimethane

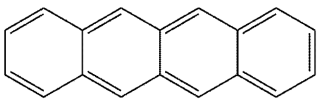

tetracene

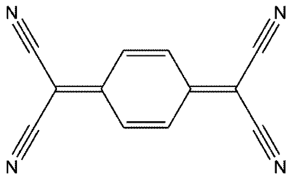

7,7,8,8-tetracyanoquinodimethane (TCNQ)

previously.[14] In our study, we initially investigated this cocrystal at 215 K and observed a *monoclinic* structure. The two structures have very similar crystal packing. Later, X-ray analysis as well as Raman spectral studies were carried out for the same crystal at several temperatures to demonstrate the phase transition between the polymorphs. In addition, both modifications were calculated with the periodic density functional theory (DFT) method to compare their crystal energies and to assess the ability of theoretical methods to predict molecular and crystal geometries of CT complexes.

EXPERIMENTAL SECTION

Preparation of Materials. Tetracene with 99% purity and TCNQ were purchased from Sigma-Aldrich. In order to remove the already-oxidized tetracene and side products, all initial materials were purified using an open system physical vapor transport (PVT) method[15] in flowing argon gas with a flow rate of 40 mL/min. A two-zone semitransparent furnace was used for single-crystal growth. The purified compounds were placed in the high-temperature zone of the furnace. The temperatures controlled by two thermocouples were set to 220 and 160 °C for the high and low-temperature zones, respectively. This temperature gradient was applied by resistive heating of two heater coils around the tubes. The inner tube in which the crystallization takes place has a diameter of 10 mm, and the outer furnace tube has a diameter of 19 mm. To avoid hydrolyzation of cyano-nitrile groups of TCNQ,[16] the inner tube was properly cleaned (using water, acetone, and alcohol) and baked out in argon flow in order to remove water and other solvents. The total growth time was around 4−5 h.

X-ray Structure Determination. The X-ray experiments were done at several temperatures. Initially the sample was slowly cooled down to 250 K for the first X-ray diffraction experiment. Data collection was then repeated at the temperatures 215, 200, 150, 125, and 100 K. Each temperature was reached by slow cooling (10 K/h) to let the structure relax and in an attempt to keep uniformity of the crystal during the phase transition. Nevertheless, the quality of the crystal deteriorated somewhat as the temperature approached that of the phase transition. According to our results, the phase transition occurs in the temperature range between 150 and 200 K without destruction of the single crystalline sample (conversion to polycrystalline or powder sample) but with the appearance of some twinning. At 200 K the structure is monoclinic with space group $C2/m$, while at 150 K and at lower temperatures the structure has triclinic symmetry with space group $P\bar{1}$. After reaching the lowest temperature of 100 K, the temperature was slowly increased, and two more experiments were done at 200 and 290 K. It is noteworthy that at temperatures of about 215−250 K the monoclinic angle β equals 90 deg; however, the structure is still monoclinic. The crystal data, data collection, and structure refinement details are summarized in Tables 1 and 2 for the monoclinic and triclinic polymorphs, respectively. Initially, the data obtained at 125 and 150 K were indexed and refined in the monoclinic crystal system. The corresponding crystallographic data and parameters of refinement are given in Table 1. However, the large errors in unit cell parameters, large *R*-factors, and analysis of residual electron density revealed that the crystal structure has triclinic symmetry at these temperatures. The comparison of the unit cell parameters for all temperatures is given in Table 3. The triclinic structures are converted to a monoclinic setting using the transformation matrix |0 −1 1| 0 −1 −1| 1 0 0|. The temperature dependence of the unit cell angles is given in Figure 1.

All experiments were carried out with a three-circle Bruker APEX-II CCD diffractometer (λ(MoK$_\alpha$)-radiation, graphite monochromator, φ and ω scan mode) and corrected for absorption.[17] The structure was determined by direct methods and refined by a full-matrix least-squares technique on F^2 with anisotropic displacement parameters for non-hydrogen atoms. The hydrogen atoms were placed in the calculated positions and refined within the riding model with fixed isotropic displacement parameters [U_{iso}(H) = 1.2U_{eq}(C)]. All calculations were carried out using the SHELXTL program.[18]

Vibrational Spectroscopy. Raman spectra of tetracene−TCNQ were taken using a Jobin-Yvon Horiba XY triple grating spectrometer over the energy range from 250 to 1550 cm^{-1} (see Figure 2 for overview) in a backscattering geometry. The sample was excited using a Melles Griot HeNe laser at 632.82 nm. The temperature was varied from 80 K to 240 K in steps of 40 K by mounting the sample in an MMR Technologies Joule−Thompson refrigerator using colloidal silver paint, with sufficient time between measurements for the sample to reach thermal equilibrium. The spectrometer was calibrated using emission lines from a Neon lamp with values from the CRC Handbook.[19] Background fluorescence and scattering were subtracted using polynomial fits, and the vibrational modes were fit to Lorentzian line shapes using a least-squares method. For assignment of major vibrational modes, M06/6-31+G(d)[20] calculations (B3LYP, 6-31G-(d,p)) were used.

Computational Details. Theoretical periodic DFT calculations of the monoclinic and triclinic crystal structures for comparison of their relative energies, unit cell parameters, and molecular geometry

DOI: 10.1021/acs.cgd.8b00501
Cryst. Growth Des. XXXX, XXX, XXX−XXX

Table 1. Selected Crystallographic Data for the Monoclinic (1a) Modification of the Cocrystal

T, K	290	250	215	200[a]	200[b]	150[c]	125[c]
a, Å	11.906(2)	11.886(3)	11.907(10)	11.869(5)	11.893(2)	11.920(14)	11.72(2)
b, Å	12.895(2)	12.858(4)	12.850(11)	12.822(6)	12.852(2)	12.839(16)	12.65(2)
c, Å	7.252(1)	7.225(2)	7.225(6)	7.195(3)	7.203(1)	7.193(9)	7.064(12)
β, °	89.847(2)	90.000(4)	90.006(10)	90.215(6)	90.192(2)	90.375(19)	90.45(3)
V	1113.3(3)	1104.1(5)	1105.5(16)	1095.0(8)	1100.9(4)	1101(2)	1047(3)
ρ_{calc}, g/cm^3	1.290	1.301	1.299	1.312	1.305	1.305	1.371
maximum theta	32.039	32.138	32.152	32.250	32.111	32.124	32.430
reflections collected	8747	6883	8833	6808	8323	6224	5691
unique reflections	1875	1928	1900	1912	1798	1851	1760
R_{int}	0.0262	0.0385	0.0344	0.0410	0.0263	0.1190	0.1434
unique reflections ($I > 2\sigma(I)$)	1322	1047	1532	1151	1459	771	462
R_1 ($I > 2\sigma(I)$)	0.0597	0.0485	0.0470	0.0488	0.0525	0.1043	0.0941
wR_2 ($I > 2\sigma(I)$)	0.1752	0.1126	0.1201	0.1167	0.1414	0.2016	0.1344

[a]Measured during the initial temperature decrease. [b]Measured during the subsequent temperature increase. [c]Initial refinement in monoclinic symmetry.

Table 2. Selected Crystallographic Data for the Triclinic (1b) Modification of the Cocrystal

T, K	150	125	100
a, Å	7.157(5)	7.149(5)	7.156(3)
b, Å	8.632(7)	8.608(6)	8.618(3)
c, Å	8.763(7)	8.777(6)	8.810(3)
α, °	85.697(13)	85.655(11)	85.648(5)
β, °	89.301(11)	89.034(10)	88.960(5)
γ, °	88.641(11)	88.302(10)	88.068(5)
V	539.7(7)	538.2(6)	541.3(3)
ρ_{calc}, g/cm^3	1.331	1.334	1.327
maximum theta	30.034	30.016	30.006
unique reflections	3099	3065	3131
unique reflections ($I > 2\sigma(I)$)	1756	1879	2528
R_1 ($I > 2\sigma(I)$)	0.0847	0.0848	0.0625
wR_2 ($I > 2\sigma(I)$)	0.2268	0.2219	0.2100

were performed using version 5.0.1 of Quantum Espresso.[21] A mix of the RRKJUS PBE pseudopotentials (PBE-RRKJUS)[22] with an energy cutoff of 816 eV was utilized. The semiempirical Grimme correction[23] was applied to take into account weak van der Waals interactions. The Brillouin zone of the reciprocal space was sampled by a Monkhorst–Pack grid: 2 × 2 × 2. The Broyden–Fletcher–Goldfarb–Shanno (BFGS) algorithm was utilized to optimize the unit cell parameters and atomic coordinates simultaneously (vc-relax option). Before the calculations, the C-centered monoclinic structure **1a** was reduced to a primitive cell (a = 7.225 Å, b = c = 8.759 Å, α = 94.37°, β = γ = 90.00°) for comparison of the results with those from the triclinic **1b** structure. The crystal structure symmetry was not fixed during optimization; however, the optimized structures had the same symmetries as the initial experimental ones. Additional calculations of crystal energy using experimental X-ray geometry were carried for both structures. For these calculations, the C–H distances were normalized to 1.09 Å. This value was taken from our calculations with optimization of the unit cell parameters and molecular geometry.

RESULTS AND DISCUSSION

The structure of the 1:1 tetracene–TCNQ cocrystal (**1a**) was unambiguously established by the X-ray diffraction study and is shown in Figure 3a along with the atomic numbering scheme. Multitemperature crystallographic studies indicated that in the temperature interval 150–200 K a transition between triclinic and monoclinic structures of the tetracene–TCNQ cocrystal occurs without destruction of the single crystal (conversion into polycrystalline or powder form) but with twinning. The cocrystal **1a** studied at higher temperatures represents a new polymorph of the tetracene–TCNQ cocrystal different from the one (**1b**) reported previously.[14] It crystallizes in the monoclinic space group $C2/m$ with both constituent molecules possessing the C_{2h} ($2/m$) symmetry (both molecules occupy special positions of $2/m$ symmetry). Interestingly, the authors of the previous work[14] mentioned that the cocrystal **1b** identified as triclinic is close to monoclinic symmetry. However, their attempts to assign higher symmetry were not successful. Indeed, the crystal structures of **1a** and **1b** are very similar but not identical. The tetracene and TCNQ molecules within the 1:1 molecular complexes are not perfectly parallel; for **1a**, their planes make an angle of 0.57(3)–0.69(2)° at temperatures 200–290 K; for **1b**, the angle is 1.87(4) ° (2.2° from literature), 1.62(6)°, and 1.32(6)° for temperatures 100, 125, and 150 K, respectively.

Furthermore, these molecules are stacked face-to-face in the same alternating manner (Figure 3b) with interplanar separations of 3.4–3.5 Å. The main difference between the structures of **1a** and **1b** is a slight rotation of the tetracene and

Table 3. Unit Cell Parameters in the Monoclinic Setting

T, K	a, Å	b, Å	c, Å	α, °	β, °	γ, °
290	11.906 (2)	12.895 (2)	7.252 (1)	90.00	89.847 (2)	90.00
250	11.886 (3)	12.858 (4)	7.225 (2)	90.00	90.000 (4)	90.00
215	11.907 (10)	12.850 (11)	7.225 (6)	90.00	90.006 (10)	90.00
200	11.893 (2)	12.852 (2)	7.203 (1)	90.00	90.192 (2)	90.00
200	11.869 (5)	12.822 (6)	7.195 (3)	90.00	90.215 (6)	90.00
150	11.830 (9)	12.753 (9)	7.157 (5)	91.400 (16)	90.474 (16)	90.869 (18)
125	11.818 (8)	12.750 (8)	7.149 (5)	91.812 (15)	90.520 (15)	91.118 (16)
100	11.847 (4)	12.783 (4)	7.156 (3)	92.019 (7)	90.632 (7)	91.261 (7)

DOI: 10.1021/acs.cgd.8b00501
Cryst. Growth Des. XXXX, XXX, XXX–XXX

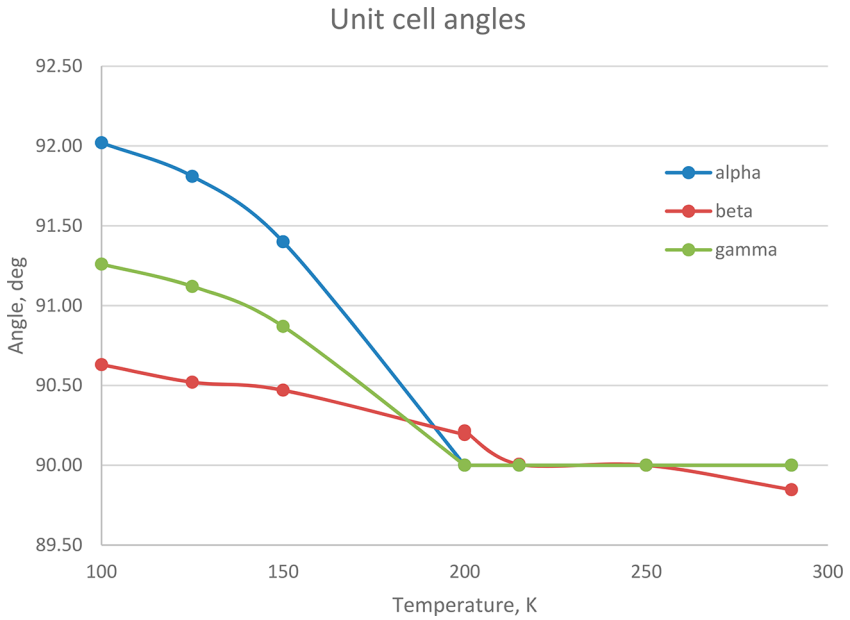

Figure 1. Temperature dependence of the unit cell angles. The values of esd are given in Table 3.

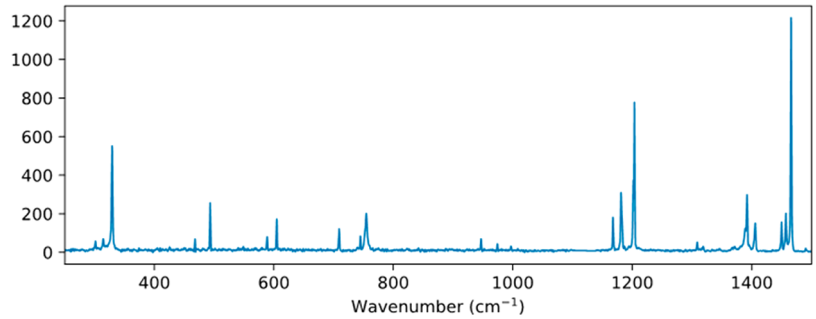

Figure 2. An overview of the Raman spectrum of tetracene–TCNQ at 80 K showing intramolecular vibrational modes.

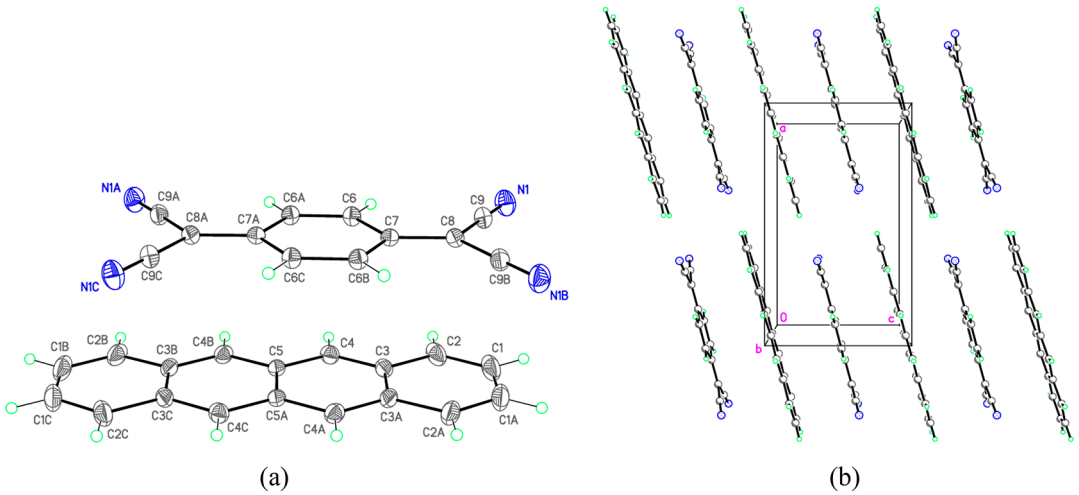

Figure 3. (a) Molecular structure of **1a**. (b) Crystal packing of **1a** demonstrating the 1:1 stacks formed by the alternating tetracene and TCNQ molecules toward [001].

TCNQ molecules by 3.1(1)° relative to each other in **1b** (the C_i ($\bar{1}$) symmetry) at 100 K, whereas the long axes of these molecules are strictly parallel in **1a** resulting in the higher C_{2h} ($2/m$) symmetry.

The periodic DFT calculations (with and without experimental geometry optimization) for both polymorphs (Table 4) revealed that structures **1a** and **1b** have energies very close to one another. The energy difference is just 0.1 and 1.1 kcal/mol for calculations with and without geometry optimization, respectively. Both types of calculations revealed that the triclinic structure **1b** has a slightly lower energy than the monoclinic structure **1a**. Static and lattice vibrational

DOI: 10.1021/acs.cgd.8b00501
Cryst. Growth Des. XXXX, XXX, XXX–XXX

Table 4. Experimental and Calculated Crystallographic Data for Structures 1a and 1b

compound	1b	calculated 1b	1a	calculated 1a
temperature, K	100		215	
crystal system	triclinic	triclinic	monoclinic	monoclinic
space group	$P\bar{1}$	$P\bar{1}$	$C2/m$	$C2/m$
a, Å	7.156(3)	6.995	11.907(1)	11.730
b, Å	8.618(3)	8.478	12.850(11)	12.620
c, Å	8.810(3)	8.714	7.225(6)	6.972
α, deg	85.648(5)	85.700	90.00	90.00
β, deg	88.960(5)	90.332	90.006(1)	92.508
γ, deg	88.068(5)	86.379	90.00	90.00
volume, Å^3	541.3(3)	514.3	1105.5(16)	1031.1
Z	1	1	2	2
ρ_{calc}, g cm^{-3}	1.327	1.397	1.299	1.393
energy for X-ray geometry, Ry/mol		−439.71178		−439.70820
energy for optimized geometry, Ry/mol		−439.73024		−439.72979

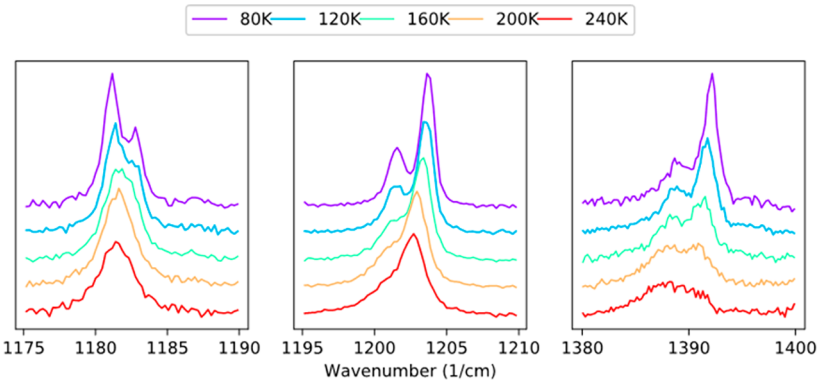

Figure 4. Splitting of vibrational modes observed at low temperatures, indicating a transition to a different structure.

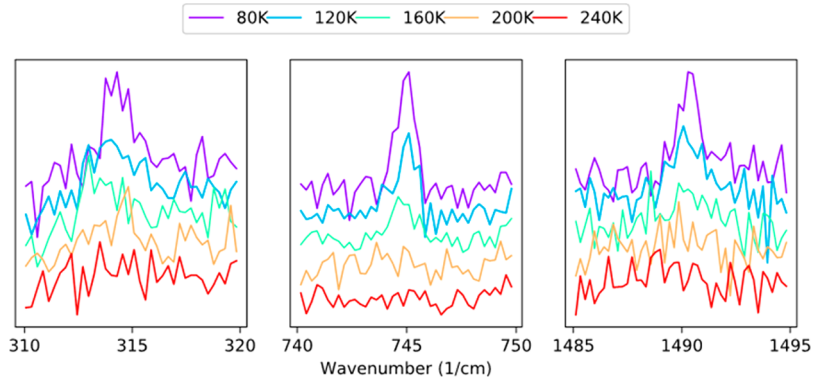

Figure 5. Examples of new Raman-active vibrational modes appearing at low temperatures, indicating a phase transition to a structure with lower symmetry.

computations of energy differences for 508 pairs of organic polymorphs demonstrated that the typical energy difference for over half of the pairs of polymorphs is less than 0.5 kcal/mol and only for 5% of the cases exceeds 1.75 kcal/mol.[24] The values reported here are therefore typical of organic crystals.

Vibrational spectroscopy measurements carried out at five temperatures from 80 to 240 K also support the occurrence of a phase transition in the complex under investigation. Splitting of the vibrational modes at 1182, 1202, 1390 cm^{-1} was observed at and below 160 K (Figure 4) in agreement with the X-ray diffraction data. In addition, the new vibrational modes at 314, 745, 1309, 1319, and 1491 cm^{-1} which were observed below the transition temperature are also in agreement with these results (see Figure 5). The degree of charge transfer was characterized using the shift in the wing C═C stretching mode of the TCNQ molecule, which is a reliable indicator.[25] The observed shift of ∼4 cm^{-1} compared to the neutral molecule corresponds (if a linear dependence is assumed) to a charge transfer value of ∼0.08, in agreement with data from XRD (see Table S1 for details). The degree of charge transfer observed in complexes **1a** and **1b** is significantly lower than for typical organic charge-transfer complexes with sulfur containing donors (e.g., tetrathiafulvalene−TCNQ or dibenzothiophene−TCNQ), but is similar to that reported for other acene−TCNQ systems.[26]

DOI: 10.1021/acs.cgd.8b00501
Cryst. Growth Des. XXXX, XXX, XXX−XXX

Since complexes **1a** and **1b** contain TCNQ acceptor molecules, the degree of charge transfer can be evaluated from the geometry of the TCNQ molecule.[27] It is known that information on the bond length alternation in the TCNQ molecule can be used to elucidate the charge transfer in a cocrystal. The main idea of these correlation methods is that the negative charge on the TCNQ molecule results in delocalization of the quinoid structure. The more-pronounced quinoid TCNQ structure corresponds to a smaller charge transfer, while the additional negative charge results in a lengthening of the shorter quinoid bonds (*a*, *c*, see Scheme 2)

Scheme 2. Notation for Alternating Bonds (a, b, c, d) in the TCNQ Molecule

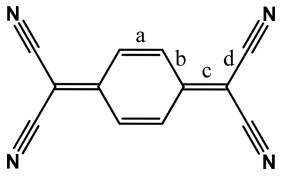

and shortening of the remaining bond lengths (*b*, *d*). Several empirical correlation schemes were proposed by different authors. We utilized the schemes proposed in ref 27a and b, Coppens and coauthors used the parameter $x = (a + c)/(b + d)$ as a measure of charge transfer (CT). This empirical scheme is based on linear interpolation between the bond lengths of pure TCNQ (no charge transfer) and the Rb TCNQ salt (one electron transferred to TCNQ). The obtained correlation is $CT = 23.81x - 22.43$. Kistenmacher and coauthors suggested to use the parameter $x = c/(b + d)$ and the correlation $CT = 41.61x - 19.81$, which is based on interpolation between the experimental CT (obtained from X-ray diffuse scattering and Bader charge analysis of experimental electron density) and geometry in eight compounds. We applied both schemes for our experimentally studied and calculated structures (Table 5), and they give very similar results. Assuming that the charge transfer does not depend on temperature (the D−A distances are almost the same in all experiments, and charge transfer from Raman spectra is also temperature-independent), the average charge transfer values can be calculated. These average values are 0.20 for the Kistenmacher scheme, and 0.18 for the Coppens scheme. These values are slightly larger than the value of 0.08 obtained from the Raman spectra. Such a discrepancy can be caused by inaccuracy of the models used to estimate the charge transfer from Raman spectra and X-ray bond lengths. An uncertainty of 0.1 (due to the crystal field effect) is reported in ref 25 for the charge transfer calculated from Raman spectra. For the X-ray models, the estimated value of charge transfer is very sensitive to the bond lengths. While the accuracy of the bond lengths in our X-ray experiments is reasonable for a standard experiment (0.002−0.006 Å), it is large enough to introduce an uncertainty of about 0.15 for the charge transfer (the charge transfer varies from 0.14 to 0.28 for the Kistenmacher scheme and from 0.16 to 0.30 for the Coppens scheme). A similar uncertainty for the charge transfer was reported in the original Coppens paper for the TTF−TCNQ cocrystal,[27a] in which the calculated charge transfer varies from 0.21 to 0.45. We therefore regard the charge transfer values obtained using the two types of measurements to be in agreement. These observations are also in agreement with the charge transfer obtained for three crystals of perylene−TCNQ with a stoichiometry 1:1, 2:1, and 3:1, for which the charge transfer ranges from 0.04 to 0.17 (Raman spectroscopic data) and from 0.01 to 0.23 from TCNQ bond length distribution data.[6a] In the same publication it was mentioned that the uncertainty of the spectroscopic evaluation is at least three times lower than that of the evaluation from the bond length distribution data.

For the calculated crystal structures **1a** and **1b** (periodic boundary DFT), the bond lengths *a* and *b* are close to the corresponding experimental values, while the bond lengths *c* and *d* deviate from the experimental lengths by about 0.02 Å or more (Table 5). The calculated length *c* is larger than the experimental one, while the length *d* is shorter, describing a more delocalized structure. These circumstances result in a significantly larger calculated charge transfer parameter of 0.7 for both modifications, **1a** and **1b**. Such a value is also in agreement with the shortened calculated interplanar D−A distance 3.3 Å (compared to 3.4−3.5 Å for the experimental structures). Hence, while theoretical calculations of crystal structures reproduce the unit cell parameters well and give reasonable molecular positions, the calculated molecular geometries are not precise enough to predict effects such as charge transfer. The discrepancy between experimental and calculated molecular geometries results in a significant deviation of the charge transfer for the calculated structures

Table 5. Bond Lengths (*A*) in TCNQ Molecules, Distance between Donor and Acceptor Molecules (*A*) in crystals, and degrees of charge transfer calculated with the Kistenmacher and Coppens approaches at different temperatures

T, K	*a*	*b*	*c*	*d*	charge transfer (Kistenmacher[a])	charge transfer (Coppens[b])	D−A distance
250	1.335	1.434	1.378	1.428	0.22	0.14	3.48
215	1.352	1.437	1.384	1.429	0.28	0.30	3.48
200	1.337	1.436	1.376	1.428	0.18	0.12	3.46
150	1.332	1.425	1.369	1.426	0.17	0.13	3.44
125	1.338	1.424	1.375	1.432	0.22	0.19	3.43
100	1.348	1.441	1.377	1.431	0.14	0.16	3.43
100, ref 23	1.345	1.451	1.378	1.431	0.09	0.07	3.43
200	1.349	1.444	1.380	1.433	0.15	0.16	3.46
290	1.344	1.437	1.380	1.432	0.21	0.18	3.49
calc **1a**	1.360	1.432	1.404	1.411	0.74	0.72	3.31
calc **1b**	1.361	1.432	1.404	1.411	0.74	0.73	3.32
calc molecule in gas phase	1.351	1.444	1.381	1.425	0.22	0.24	

[a]Formula $CT = 41.61*c/(b + d) - 19.81$. [b]Formula $CT = 23.81*(a + c)/(b + d) - 22.43$.

DOI: 10.1021/acs.cgd.8b00501
Cryst. Growth Des. XXXX, XXX, XXX−XXX

in comparison with those of the experimental ones. Therefore this method cannot be recommended for prediction of charge transfer properties of complexes. Interestingly, the experimental parameters a, b, c, d and the corresponding charge transfer are in better agreement with the quantum chemical calculation (Gaussian09) of the geometry parameters of a single molecule in the gas phase (Table 5).

CONCLUSION

A multitemperature study of the tetracene−TCNQ cocrystal was carried out with X-ray diffraction and Raman spectroscopy methods. A new, monoclinic polymorph was observed at 250 K, in addition to the previously reported triclinic polymorph observed at low temperatures. Both experimental methods suggest that a phase transition between the two polymorphs occurs in the temperature interval 150−200 K. It is important to mention that the phase transition was reversible in the sense that it did not destroy the crystal but involves only small changes of molecular positions that were reflected in the change of crystal symmetry. The molecular geometry also did not change significantly. The degree of charge transfer estimated based on the TCNQ molecular geometry derived from X-ray diffraction was found to be in the interval 0.12−0.30 depending on the temperature and calculation method. The charge transfer obtained from the experimental vibrational shift in the C═C stretching mode gave a value of 0.08, which is in agreement with the result obtained from the X-ray measurements given the uncertainties in both calculations. The periodic DFT quantum chemical calculations give reasonable molecular geometries and unit cell parameters; however a more sophisticated method should be used to estimate charge transfer in such compounds. The calculated energy difference between the two polymorphs was found to be about 1.0 kcal/mol, which reflects the similarity of the two structures, as experimentally manifested in the reversibility of the phase transition.

ASSOCIATED CONTENT

Supporting Information

The Supporting Information is available free of charge on the ACS Publications website at DOI: 10.1021/acs.cgd.8b00501.

Table 1: Degree of charge transfer in tetracene−TCNQ estimated from the shift in the C═C wing modes of TCNQ. Table 2: List of the major Raman active vibrational modes in tetracene−TCNQ as with details about the motion (PDF)

Accession Codes

CCDC 1507751, 1837360−1837362, and 1837364−1837367 contain the supplementary crystallographic data for this paper. These data can be obtained free of charge via www.ccdc.cam.ac.uk/data_request/cif, or by emailing data_request@ccdc.cam.ac.uk, or by contacting The Cambridge Crystallographic Data Centre, 12 Union Road, Cambridge CB2 1EZ, UK; fax: +44 1223 336033.

AUTHOR INFORMATION

Corresponding Author

*E-mail: tvtimofeeva@nmhu.edu.

ORCID

Victor N. Khrustalev: 0000-0001-8806-2975

Laurie E. McNeil: 0000-0001-8926-9548

Tatiana V. Timofeeva: 0000-0001-7475-3206

Notes

The authors declare no competing financial interest.

ACKNOWLEDGMENTS

This work was supported by NSF via DMR-1523611 (PREM) and DMR-1708379. The authors also gratefully acknowledge the Ohio Supercomputer Center for providing computational resources and Dr. D. Pelekhov (OSU CEM) for help with computations.

REFERENCES

(1) (a) Fan, J.; Zhang, Y.; Lang, C.; Qiu, M.; Song, J.; Yang, R.; Guo, F.; Yu, Q.; Wang, J.; Zhao, L. Side chain effect on poly(beznodithiophene-co-dithienobenzoquinoxaline) and their applications for polymer solar cells. *Polymer* **2016**, *82*, 228−237. (b) Mondal, R.; Miyaki, N.; Becerril, H. A.; Norton, J. E.; Parmer, J.; Mayer, A. C.; Tang, M. L.; Brédas, J.-L.; McGehee, M. D.; Bao, Z. Synthesis of Acenaphthyl and Phenanthrene Based Fused-Aromatic Thienopyrazine Co-Polymers for Photovoltaic and Thin Film Transistor Applications. *Chem. Mater.* **2009**, *21* (15), 3618−3628. (c) Keshtov, M. L.; Kuklin, S. A.; Radychev, N. A.; Nikolaev, A. Y.; Ostapov, I. E.; Krayushkin, M. M.; Konstantinov, I. O.; Koukaras, E. N.; Sharma, A.; Sharma, G. D. New low bandgap near-IR conjugated D-A copolymers for BHJ polymer solar cell applications. *Phys. Chem. Chem. Phys.* **2016**, *18* (12), 8389−8400. (d) Zhang, Y.; Zou, J.; Yip, H.-L.; Chen, K.-S.; Davies, J. A.; Sun, Y.; Jen, A. K. Y. Synthesis, Characterization, Charge Transport, and Photovoltaic Properties of Dithienobenzoquinoxaline- and Dithienobenzopyridopyrazine-Based Conjugated Polymers. *Macromolecules* **2011**, *44* (12), 4752−4758.

(2) Sosorev, A. Y.; Paraschuk, D. Y. Charge-Transfer Complexes of Conjugated Polymers. *Isr. J. Chem.* **2014**, *54* (5−6), 650−673.

(3) Chung, H.; Diao, Y. Polymorphism as an emerging design strategy for high performance organic electronics. *J. Mater. Chem. C* **2016**, *4* (18), 3915−3933.

(4) Guo, S.; Mohapatra, S. K.; Romanov, A.; Timofeeva, T. V.; Hardcastle, K. I.; Yesudas, K.; Risko, C.; Brédas, J.-L.; Marder, S. R.; Barlow, S. n-Doping of Organic Electronic Materials Using Air-Stable Organometallics: A Mechanistic Study of Reduction by Dimeric Sandwich Compounds. *Chem. - Eur. J.* **2012**, *18* (46), 14760−14772.

(5) Jiang, H.; Hu, P.; Ye, J.; Zhang, K. K.; Long, Y.; Hu, W.; Kloc, C. Tuning of the degree of charge transfer and the electronic properties in organic binary compounds by crystal engineering: a perspective. *J. Mater. Chem. C* **2018**, *6* (8), 1884−1902.

(6) (a) Vermeulen, D.; Zhu, L. Y.; Goetz, K. P.; Hu, P.; Jiang, H.; Day, C. S.; Jurchescu, O. D.; Coropceanu, V.; Kloc, C.; McNeil, L. E. Charge Transport Properties of Perylene−TCNQ Crystals: The Effect of Stoichiometry. *J. Phys. Chem. C* **2014**, *118* (42), 24688−24696. (b) Salzillo, T.; Masino, M.; Kociok-Köhn, G.; Di Nuzzo, D.; Venuti, E.; Della Valle, R. G.; Vanossi, D.; Fontanesi, C.; Girlando, A.; Brillante, A.; Da Como, E. Structure, Stoichiometry, and Charge Transfer in Cocrystals of Perylene with TCNQ-Fx. *Cryst. Growth Des.* **2016**, *16* (5), 3028−3036.

(7) (a) Mori, T.; Inokuchi, H. Crystal Structure of the Mixed-Stacked Salt of Bis(ethylenedithio)tetrathiafulvalene (BEDT-TTF) and Tetracyanoquinodimethane (TCNQ). *Bull. Chem. Soc. Jpn.* **1987**, *60* (1), 402−404. (b) Mori, T.; Inokuchi, H. Structural and electrical properties of (BEDT-TTF)(TCNQ). *Solid State Commun.* **1986**, *59* (6), 355−359. (c) Mori, T.; Kawamoto, T. Organic conductors-from fundamentals to nonlinear conductivity. *Annu. Rep. Prog. Chem., Sect. C: Phys. Chem.* **2007**, *103*, 134−172.

(8) Goetz, K. P.; Tsutsumi, J.; Pookpanratana, S.; Chen, J.; Corbin, N. S.; Behera, R. K.; Coropceanu, V.; Richter, C. A.; Hacker, C. A.; Hasegawa, T.; Jurchescu, O. D. Polymorphism in the 1:1 Charge-Transfer Complex DBTTF−TCNQ and Its Effects on Optical and Electronic Properties. *Advanced Electronic Materials* **2016**, *2* (10), 1600203.

DOI: 10.1021/acs.cgd.8b00501
Cryst. Growth Des. XXXX, XXX, XXX−XXX

(9) Sato, O. Dynamic molecular crystals with switchable physical properties. *Nat. Chem.* **2016**, *8*, 644.
(10) Goetz, K. P.; Fonari, A.; Vermeulen, D.; Hu, P.; Jiang, H.; Diemer, P. J.; Ward, J. W.; Payne, M. E.; Day, C. S.; Kloc, C.; Coropceanu, V.; McNeil, L. E.; Jurchescu, O. D. Freezing-in orientational disorder induces crossover from thermally-activated to temperature-independent transport in organic semiconductors. *Nat. Commun.* **2014**, *5*, 5642.
(11) Horiuchi, S.; Tokura, Y. Organic ferroelectrics. *Nat. Mater.* **2008**, *7*, 357−366.
(12) Benmansour, S.; Marchivie, M.; Triki, S.; Gómez-García, C. J. Polymorphism and Metallic Behavior in BEDT-TTF Radical Salts with Polycyano Anions. *Crystals* **2012**, *2* (2), 306−326.
(13) Bernstein, J.; Davey, R. J.; Henck, J.-O. Concomitant Polymorphs. *Angew. Chem., Int. Ed.* **1999**, *38* (23), 3440−3461.
(14) Buurma, A. J. C.; Jurchescu, O. D.; Shokaryev, I.; Baas, J.; Meetsma, A.; de Wijs, G. A.; de Groot, R. A.; Palstra, T. T. M. Crystal Growth, Structure, and Electronic Band Structure of Tetracene−TCNQ. *J. Phys. Chem. C* **2007**, *111* (8), 3486−3489.
(15) Laudise, R. A.; Kloc, C.; Simpkins, P. G.; Siegrist, T. Physical vapor growth of organic semiconductors. *J. Cryst. Growth* **1998**, *187* (3), 449−454.
(16) Vollhardt, K. P. C.; Schore, N. E. *Organic Chemistry: Structure and Function*, 3rd ed.; Freeman: New York, 1998.
(17) Sheldrick, G. M. *SADABS, v. 2.03, Bruker/Siemens Area Detector Absorption Correction Program*; Bruker AXS Inc.: Madison, WI, 2003.
(18) Sheldrick, G. Crystal structure refinement with SHELXL. *Acta Crystallogr., Sect. C: Struct. Chem.* **2015**, *71* (1), 3−8.
(19) Rumble, J. R.; Rumble, J. *CRC Handbook of Chemistry and Physics*, 98th ed.; CRC Press LLC: Boca Raton, FL, 2017.
(20) Frisch, M. J.; Trucks, G. W.; Schlegel, H. B.; Scuseria, G. E.; Robb, M. A.; Cheeseman, J. R.; Scalmani, G.; Barone, V.; Mennucci, B.; Petersson, G. A.; Nakatsuji, H.; Caricato, M.; Li, X.; Hratchian, H. P.; Izmaylov, A. F.; Bloino, J.; Zheng, G.; Sonnenberg, J. L.; Hada, M.; Ehara, M.; Toyota, K.; Fukuda, R.; Hasegawa, J.; Ishida, M.; Nakajima, T.; Honda, Y.; Kitao, O.; Nakai, H.; Vreven, T.; Montgomery, J. A., Jr.; Peralta, J. E.; Ogliaro, F.; Bearpark, M.; Heyd, J. J.; Brothers, E.; Kudin, K. N.; Staroverov, V. N.; Kobayashi, R.; Normand, J.; Raghavachari, K.; Rendell, A.; Burant, J. C.; Iyengar, S. S.; Tomasi, J.; Cossi, M.; Rega, N.; Millam, J. M.; Klene, M.; Knox, J. E.; Cross, J. B.; Bakken, V.; Adamo, C.; Jaramillo, J.; Gomperts, R.; Stratmann, R. E.; Yazyev, O.; Austin, A. J.; Cammi, R.; Pomelli, C.; Ochterski, J. W.; Martin, R. L.; Morokuma, K.; Zakrzewski, V. G.; Voth, G. A.; Salvador, P.; Dannenberg, J. J.; Dapprich, S.; Daniels, A. D.; Farkas, O.; Foresman, J. B.; Ortiz, J. V.; Cioslowski, J.; Fox, D. J. *Gaussian 09*; Gaussian, Inc.: Wallingford, CT, 2009.
(21) Giannozzi, P.; Baroni, S.; Bonini, N.; Calandra, M.; Car, R.; Cavazzoni, C.; Ceresoli, D.; Chiarotti, G. L.; Cococcioni, M.; Dabo, I.; Dal Corso, A.; de Gironcoli, S.; Fabris, S.; Fratesi, G.; Gebauer, R.; Gerstmann, U.; Gougoussis, C.; Kokalj, A.; Lazzeri, M.; Martin-Samos, L.; Marzari, N.; Mauri, F.; Mazzarello, R.; Paolini, S.; Pasquarello, A.; Paulatto, L.; Sbraccia, C.; Scandolo, S.; Sclauzero, G.; Seitsonen, A. P.; Smogunov, A.; Umari, P.; Wentzcovitch, R. M. QUANTUM ESPRESSO: a modular and open-source software project for quantum simulations of materials. *J. Phys.: Condens. Matter* **2009**, *21* (39), 395502 1−19.
(22) Rappe, A. M.; Rabe, K. M.; Kaxiras, E.; Joannopoulos, J. D. Optimized pseudopotentials. *Phys. Rev. B: Condens. Matter Mater. Phys.* **1990**, *41* (2), 1227−1230.
(23) (a) Grimme, S. Semiempirical GGA-type density functional constructed with a long-range dispersion correction. *J. Comput. Chem.* **2006**, *27* (15), 1787−1799. (b) Barone, V.; Casarin, M.; Forrer, D.; Pavone, M.; Sambi, M.; Vittadini, A. Role and effective treatment of dispersive forces in materials: Polyethylene and graphite crystals as test cases. *J. Comput. Chem.* **2009**, *30* (6), 934−939.
(24) Nyman, J.; Day, G. M. Static and lattice vibrational energy differences between polymorphs. *CrystEngComm* **2015**, *17* (28), 5154−5165.
(25) Matsuzaki, S.; Kuwata, R.; Toyoda, K. Raman spectra of conducting TCNQ salts; Estimation of the degree of charge transfer from vibrational frequencies. *Solid State Commun.* **1980**, *33* (4), 403−405.
(26) (a) Williams, R. M.; Wallwork, S. C. Molecular complexes exhibiting polarization bonding. XI. The crystal and molecular structure of the 7,7,8,8-tetracyanoquinodimethane-anthracene complex. *Acta Crystallogr., Sect. B: Struct. Crystallogr. Cryst. Chem.* **1968**, *24* (2), 168−174. (b) Shaanan, B.; Shmueli, U.; Rabinovich, D. Structure and packing arrangement of molecular compounds. VII. 7,7,8,8-Tetracyanoquinodimethane-naphthalene (1:1). *Acta Crystallogr., Sect. B: Struct. Crystallogr. Cryst. Chem.* **1976**, *32* (9), 2574−2580. (c) Prout, C. K.; Tickle, I. J.; Wright, J. D. Molecular complexes. Part XVI. Crystal structure of the 1:1 molecular complex of pyrene and 7,7,8,8-tetracyanoquinodimethane. *J. Chem. Soc., Perkin Trans. 2* **1973**, No. 5, 528−530. (d) Tickle, I. J.; Prout, C. K. Molecular complexes. Part XVII. Crystal and molecular structure of perylene-7,7,8,8-tetracyanoquinodimethane molecular complex. *J. Chem. Soc., Perkin Trans. 2* **1973**, No. 6, 720−723. (e) Munnoch, P. J.; Wright, J. D. Crystal structure of the 1:1 molecular complex of chrysene and 7,7,8,8-tetracyanoquinodimethane. *J. Chem. Soc., Perkin Trans. 2* **1974**, No. 11, 1397−1400. (f) Chi, X.; Besnard, C.; Thorsmølle, V. K.; Butko, V. Y.; Taylor, A. J.; Siegrist, T.; Ramirez, A. P. Structure and Transport Properties of the Charge-Transfer Salt Coronene−TCNQ. *Chem. Mater.* **2004**, *16* (26), 5751−5755. (g) Dobrowolski, M. A.; Garbarino, G.; Mezouar, M.; Ciesielski, A.; Cyranski, M. K. Structural diversities of charge transfer organic complexes. Focus on benzenoid hydrocarbons and 7,7,8,8-tetracyanoquinodimethane. *CrystEngComm* **2014**, *16* (3), 415−429.
(27) (a) Coppens, P.; Row, T. N. G. X-Ray Diffraction Measurement of Net Atomic and Molecular Charges. *Ann. N. Y. Acad. Sci.* **1978**, *313* (1), 244−255. (b) Kistenmacher, T. J.; Emge, T. J.; Bloch, A. N.; Cowan, D. O. Structure of the red, semiconducting form of 4,4',5,5'-tetramethyl-[Delta]2,2'-bi-1,3-diselenole-7,7,8,8-tetracyano-p-quinodimethane, TMTSF-TCNQ. *Acta Crystallogr., Sect. B: Struct. Crystallogr. Cryst. Chem.* **1982**, *38* (4), 1193−1199. (c) Flandrois, S.; Chasseau, D. Longueurs de liaison et transfert de charge dans les sels du tetracyanoquinodimethane (TCNQ). *Acta Crystallogr., Sect. B: Struct. Crystallogr. Cryst. Chem.* **1977**, *33* (9), 2744−2750.

DOI: 10.1021/acs.cgd.8b00501
Cryst. Growth Des. XXXX, XXX, XXX−XXX